Instantaneous and time-averaged velocity fields in a wide electrostatic precipitator

J. Podlinski, Pierre Atten, J. Mizeraczyk

6ème Conférence de la Société Française d'Electrostatique, Paris & Gif-sur-Yvette, 8-9 juillet 2008, ISBN : 978-2-9505432-6-4, pp. 142-149 (2008)

Instantaneous and time-averaged velocity fields in a wide electrostatic precipitator

Janusz Podliński, Pierre Atten, Jerzy Mizeraczyk

***Abstract*— This work was aimed at clarifying whether the electrohydrodynamic (EHD) flow in a relatively wide electrostatic precipitator (ESP) (width:height = 2) is 2- or 3-dimensional (3D). The previous our measurements of 3D time-averaged flow velocity fields suggested that the flow in the ESP duct centre is almost 2-dimensional. In this paper we present both the 3D instantaneous and time-averaged flow velocity fields in a relatively wide ESP (width:height = 2). The ESP used in this work was an acrylic parallelepiped with a negatively polarized wire discharge electrode and two plate collecting electrodes. The velocity field was measured using Particle Image Velocimetry in the observation midplane along the ESP.**

***Index Terms* — electrohydrodynamic flow, EHD, electrostatic precipitator, ESP, Particle Image Velocimetry.**

I. Introduction

THE fine dust particles emitted by industry and transportation means can contain substances harmful to human health, such as oxides of sulphur, nitric oxides, ammonia and heavy metals. The most dangerous for health are dusts with the diameter of grains below 2.5 μm (fraction called PM2.5), which can penetrate from lungs directly to blood. Therefore, in the last years in the European Union a special attention to the inspection of emission of fine dust particles of micron and submicron sizes increased. The European Parliament is preparing the new directive concerning the quality of air in the European Union [1, 2].

The industry, in particular the heat and power industry based on coal fuel, is a major source of fine dust particle emission. For several decades the heat and power plants are equipped with filters to reduce dust emission. Most popular are electrostatic precipitators (ESPs) which are basic devices for the reduction of dust emission. The total mass collection efficiency of dust in modern ESPs is very high (above 99%), however the collection efficiency of micron and submicron dust particle is much lower (below 80%) and still unsatisfactory [3]. It means that a large number of fine particles is emitted to the atmosphere, becoming dangerous to people and animals.

The precipitation of particles in the ESP duct depends on the dust-particle properties, electric field, electric space charge and gas flow field [4]. The primary gas flow (that entering the ESP) is disturbed by the electrohydrodynamic (EHD) secondary flow generated in the ESP. The EHD secondary flow causes considerable changes and turbulences in the primary flow structures. Influence of the EHD secondary flow on the ESP collection efficiency has been debated for decades. To elucidate this influence many experimental [5-11] and numerical [12-14] investigations were carried out. Some of the results showed that the EHD secondary flow and corresponding gas flow turbulences are important for collecting fine dust particles in ESPs [11, 12].

In this paper, the results of 3-dimensional Particle Image Velocimetry (3D PIV) [15] measurements of the flow velocity fields in a relatively wide wire-plate type ESP are presented. The measurements were carried out in the observation midplane along the ESP.

II. Experiment

The apparatus used in this experiment consisted of an ESP, DC high voltage supply and a standard 3D Particle Image Velocimetry (PIV) equipment for the flow velocity field measurement (Fig. 1).

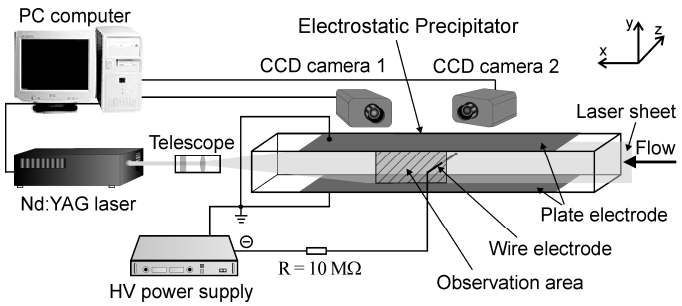

Fig. 1. Experimental set-up for 3D-PIV flow velocity field measurements in ESP.

Manuscript received on May 30, 2008. This work was supported in part by the Polish Ministry of Science under Grant 1857/B/T02/2007/33.

J. Podliński is with the Centre for Plasma and Laser Engineering, The Szewalski Institute of Fluid Flow Machinery, Polish Academy of Sciences (IFFM PAS), Fiszera 14, 80-952 Gdańsk, Poland (phone: +4858 6995122; fax: +4858 3416144; e-mail: janusz@imp.gda.pl).

P. Atten is with the G2Elab, CNRS, INP Grenoble and Joseph Fourier University, BP 166, 38042 Grenoble Cedex 9, France.

J. Mizeraczyk is with the Centre for Plasma and Laser Engineering, The Szewalski Institute of Fluid Flow Machinery, Polish Academy of Sciences (IFFM PAS), Fiszera 14, 80-952 Gdańsk, Poland and with the Department of Marine Electronics, Gdynia Maritime University, Gdynia, Poland.

The wide-type ESP used in this work was an acrylic parallelepiped 1000 mm long, 200 mm wide and 100 mm high (width:height = 2). The electrical electrode set consisted of a wire discharge electrode and two collecting plate electrodes. The wire electrode (diameter 1 mm, length 200 mm) was placed perpendicularly to the main flow, in the middle of the ESP between the plate electrodes, which were placed on the top and bottom of the ESP. The width of each plate electrodes was 200 mm, while the plate-to-plate electrode spacing was 100 mm. A flow homogenizer was placed before the ESP inlet.

Air flow seeded with a cigarette smoke (majority of smoke particles lower than 1 μm in dry air) was blown along the reactor duct with an average velocity (from 0 to 0.9 m/s). The negative DC voltage of up to 28 kV was applied to the wire electrode through a 10 MΩ resistor, while the plate electrodes were grounded. The averaged discharge current was up to 150 μA.

The standard 3D PIV equipment consisted of a twin second harmonic Nd-YAG laser system (λ = 532 nm), imaging optics (cylindrical telescope), two CCD cameras and a PC computer with Dantec FlowManager software.

The 3D PIV measurements were carried out in a plane placed perpendicularly to both electrodes, at the wire electrode midpoint. The observation area (the area of the laser sheet "seen" by both CCD cameras) covered a region between the plate electrodes, ranging from 20 mm towards the flow upstream direction to 205 mm towards the flow downstream direction, when measured from the wire electrode (Fig. 1).

The results obtained from 3D PIV measurements are presented in this paper among other things as vector maps and colour maps. The vector maps (called flow velocity fields) show velocity x- and y-component. The colour maps show velocity z-component.

III. Results

Figs. 2–6 show the results of the 3D PIV measurements in the ESP when no voltage was applied. The Reynolds number was $Re = V \times L / \nu = 5730$ [16]. The parameters used to calculate Re were: the primary flow average velocity V = 0.9 m/s, the characteristic length (plate-plate distance) L = 0.1 m, and the air kinematic viscosity $\nu = 1.57 \times 10^{-5}$ m^2/s).

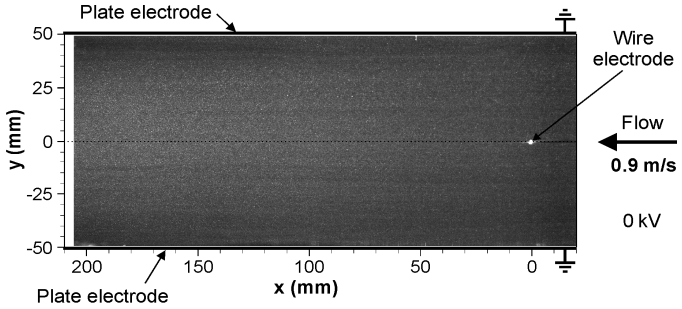

Fig. 2. Instantaneous image of the flow in the ESP when no voltage was applied. The primary flow average velocity was 0.9 m/s. Exposure time: 6 ns.

Fig. 2 shows a typical single image of the flow in the ESP taken by the CCD camera. The dust particles scattering the laser light are visible as bright points in the image. When no voltage was applied, the submicron dust particles followed the gas main flow and, in this case, the measured velocity field of the particles corresponds to the gas flow velocity field. Figs. 3 and 4 show the particle flow velocity field resulted from averaging of 100 PIV images, which means that the velocity field is time-averaged. Based on the measured velocity fields, the velocity standard deviation for the x-component (Fig. 5) and the z-component (Fig. 6) was determined.

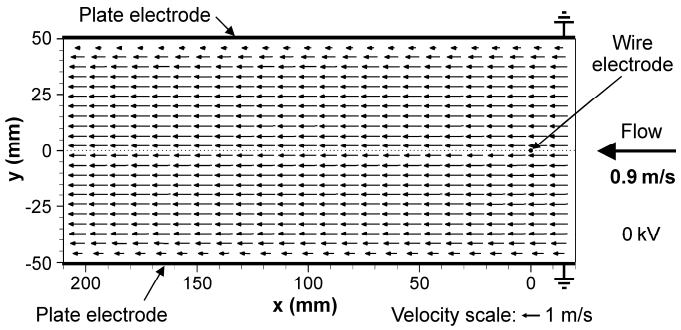

Fig. 3. Averaged flow velocity field in the ESP when no voltage was applied. The primary flow average velocity was 0.9 m/s.

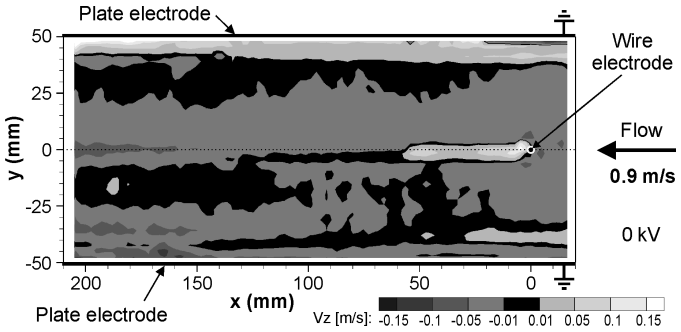

Fig. 4. Averaged flow velocity z-component in the ESP when no voltage was applied. The primary flow average velocity was 0.9 m/s.

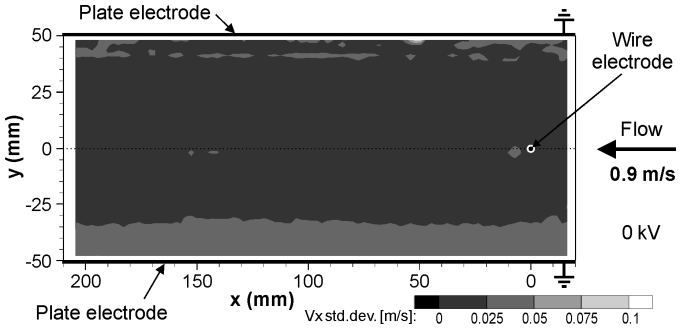

Fig. 5. Standard deviation of velocity x-component in the ESP when no voltage was applied. The primary flow average velocity was 0.9 m/s.

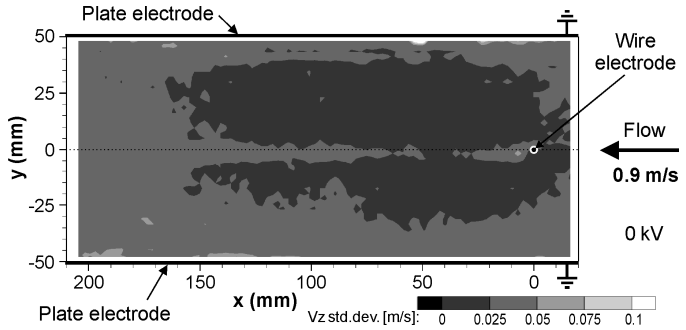

Fig. 6. Standard deviation of velocity z-component in the ESP when no voltage was applied. The primary flow average velocity was 0.9 m/s.

It is clearly seen from the presented figures that the flow was laminar. The standard deviation of the velocity x-component was very low (lower than 0.035 m/s). Small disturbances of the flow were found in the wake behind the wire electrode. The average velocity z-component was very low (lower than 0.05 m/s in the + and – z direction). Its standard deviation was very low (Figs. 4 and 6). It means that the flow was practically 2-dimensional in the observation area when no voltage was applied.

It is worth mentioning that the flow velocity patterns measured for the primary flow average velocity of 0.2 m/s and 0.6 m/s (not shown in this paper), when no voltage was applied, were very similar to that for the primary flow average velocity of 0.9 m/s.

When a high voltage was applied to the wire electrode, the electric forces exerted by the corona discharge and electric field induce a considerable EHD secondary flow of the gas which altered significantly the primary laminar flow. On another hand, the electric force exerted on each individual dust particle with charge q_p induces a drift of the particle with respect to the suspending air. Therefore, the net motion of the charged dust particles has two components, one due to the gas flow and the other, due to the electric force $q_p\boldsymbol{E}$ (the particle drift velocity), where $\boldsymbol{E}$ is the electric field. For submicron particles, except just around the wire electrode (where $\boldsymbol{E}$ is very high), the particle drift velocity is much lower than the gas velocity [4]. Therefore, we can assume that also the charged dust particles follow the gas flow. Hence, the measured by us particle flow velocity fields represent also the gas flow velocity fields in the ESP, except for the near-wire region.

Figs. 7–15 show the time-averaged results of the 3D PIV measurements in the ESP when negative voltage of 28 kV was applied. The average total discharge current was 150 μA. At this current, the EHD number, which is related to the electric forces, was 5×10^7. The EHD number was calculated using a formula: $\mathrm{Ehd} = I \times L^3 / (\nu^2 \times \rho \times \mu_i \times A)$ [16], with the parameters as follows: $I = 150\ \mu A$ (the average total discharge current), $L = 0.1$ m (the distance between the collecting electrodes), $\nu = 1.57 \times 10^{-5}\ m^2/s$ (the air kinematic viscosity), $\rho = 1.205\ kg/m^3$ (the air density), $A = 0.04\ m^2$ (the discharge area) and $\mu_i = 2.55 \times 10^{-4}\ m^2/Vs$ (the ion mobility).

The particle flow velocity field and the corresponding flow streamlines in the ESP for 28 kV and 0.9 m/s are presented in Figs. 7-9. The Reynolds number was Re = 5730, the EHD number was 5×10^7, and the ratio of the EHD number to the Reynolds number squared was 1.5 ($\mathrm{Ehd/Re^2}$ describes the ratio of the electric forces to the inertial force). For this relatively low $\mathrm{Ehd/Re^2}$ ratio the influence of the discharge on the dust particle trajectories is mostly seen in the discharge region, i.e. in a radius of about 50 mm from the wire electrode. As can be seen in Figs. 7 and 8, the particle trajectories are bent towards the plate electrodes in this region. The average velocity z-component (Fig. 9) in almost whole observation

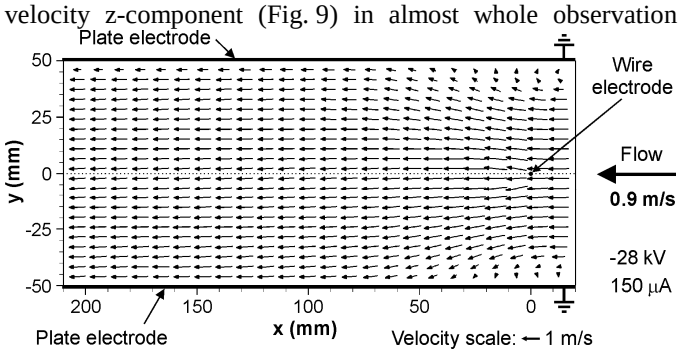

Fig. 7. Averaged flow velocity field in the ESP. The applied voltage was -28 kV. The primary flow average velocity was 0.9 m/s.

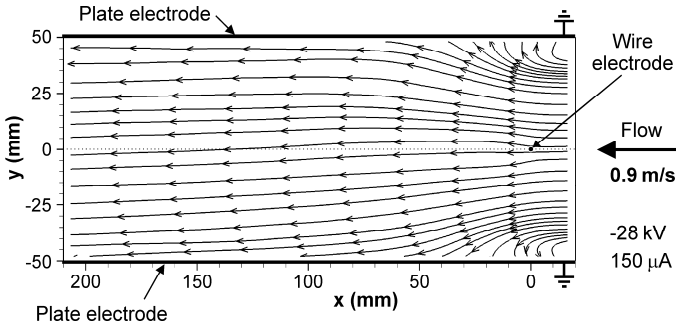

Fig. 8. Flow streamlines in the ESP. The applied voltage was -28 kV. The primary flow average velocity was 0.9 m/s.

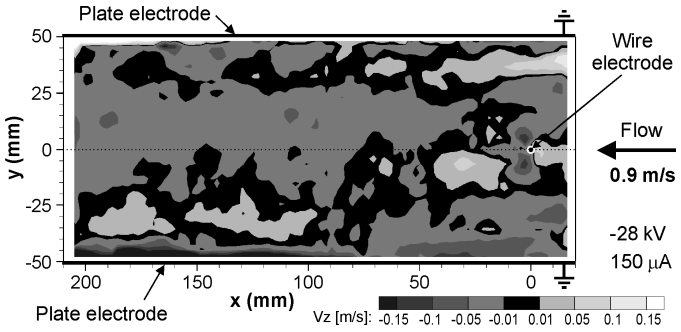

Fig. 9. Averaged flow velocity z-component in the ESP. The applied voltage was -28 kV. The primary flow average velocity was 0.9 m/s.

area was very low (lower than 0.05 m/s), increasing near the wire electrode and plate electrodes up to 0.15 m/s.

When the primary flow average velocity decreased to 0.6 m/s (Figs. 10-12), the Reynolds number decreased to 3820 and the ratio $\mathrm{Ehd/Re^2}$ increased to 3.4. Under these conditions the influence of the discharge on the dust particle motion is

a stronger than that at 0.9 m/s (Figs. 7-9). The particle trajectories bent stronger towards the collecting electrodes. The velocity y-component increased in the discharge region. The average velocity z-component is still very low (lower than 0.05 m/s).

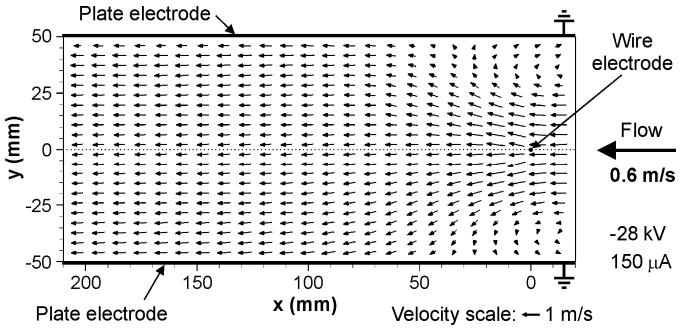

Fig. 10. Averaged flow velocity field in the ESP. The applied voltage was -28 kV. The primary flow average velocity was 0.6 m/s.

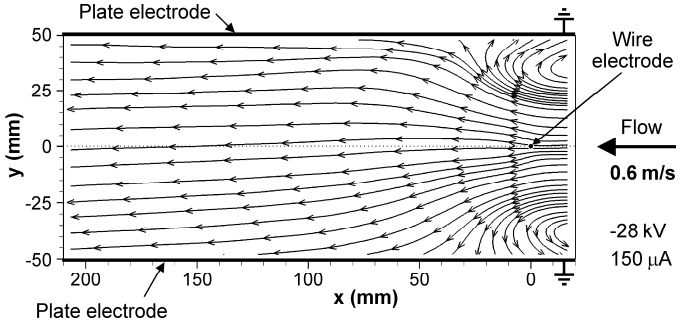

Fig. 11. Flow streamlines in the ESP. The applied voltage was -28 kV. The primary flow average velocity was 0.6 m/s.

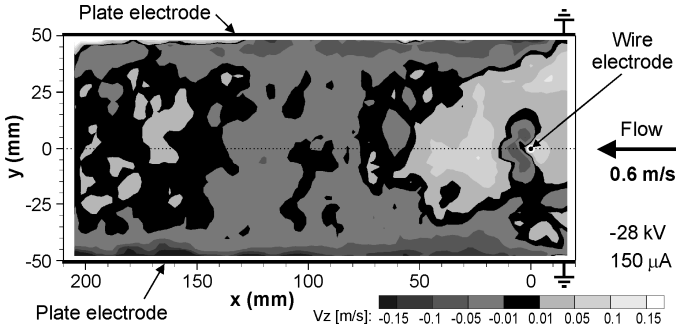

Fig. 12. Averaged flow velocity z-component in the ESP. The applied voltage was -28 kV. The primary flow average velocity was 0.6 m/s.

For a still lower primary flow average velocity (0.2 m/s) (Figs. 13-15), the Reynolds number decreased to 1270 and the Ehd/Re^2 ratio increased to 30.6 (the electric forces clearly dominate over the inertial force). In consequence, the EHD secondary flow significantly changed the average velocity field in the majority of observation area. 100 mm downstream from the wire electrode a pair of vortices occurred. As a result the particle flowed in the opposite direction to the primary flow direction in the ESP duct centre. The average velocity z-component is still very low (lower than 0.05 m/s) and only near the electrodes it reaches the values up to 0.15 m/s.

As it can be seen from Figs. 7-15, the increase in Ehd/Re^2 ratio caused strong disturbances of the average velocity field, whereas the average velocity z-component was not much disturbed by the discharge and maintained almost constant small value. It means that the time-averaged flow velocity field measured in the ESP midplane as shown in Fig. 1, is almost 2-dimensional. However, we can expect that the time-averaged velocity field in the observation planes near the ESP walls are 3-dimensional due to the end-walls effect.

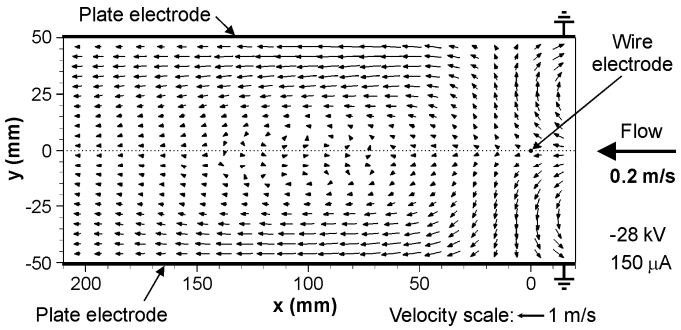

Fig. 13. Averaged flow velocity field in the ESP. The applied voltage was -28 kV. The primary flow average velocity was 0.2 m/s.

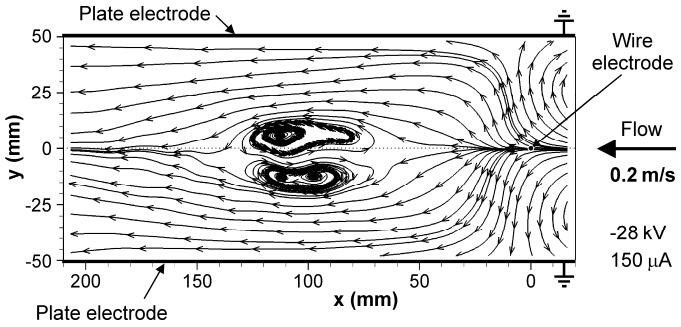

Fig. 14. Flow streamlines in the ESP. The applied voltage was -28 kV. The primary flow average velocity was 0.2 m/s.

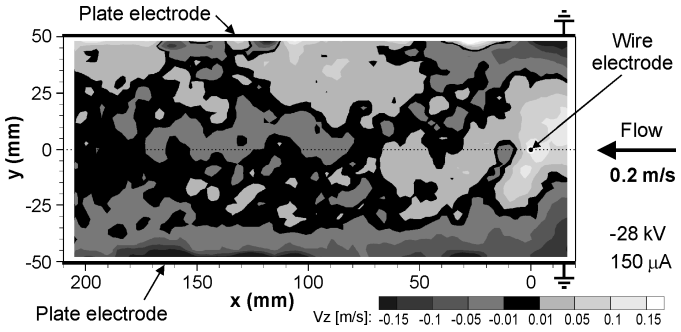

Fig. 15. Averaged flow velocity z-component in the ESP. The applied voltage was -28 kV. The primary flow average velocity was 0.2 m/s.

From the time-averaged results presented above one can conclude, that the flow in the ESP is 2-dimensional. However, our analysis of the instantaneous flow velocity fields measured by us and presented below show that the flow in the ESP is 3 dimensional when short time intervals are considered.

The instantaneous images of the particle flow and corresponding instantaneous flow velocity fields measured in the ESP for a negative voltage of 28 kV are presented in Figs. 16-24.

As it can be seen from instantaneous images shown in Fig. 16, voltage 28 kV, primary flow average velocity 0.9 m/s (Ehd/Re^2 1.5), the Karman vortex structure occurred just behind the wire electrode. However, this structure is unstable and it is scattered by irregular flow disturbances starting at the latest 40 mm downstream from the wire electrode. The corresponding instantaneous flow velocity fields (Fig. 17) as well as velocity z-component (Fig. 18) also show this irregular disturbances. In the downstream from the wire electrode quite distinct instabilities occurs for the flow velocity x- and y-component. The velocity z-component reaches values up to 0.3 m/s and even more near the plate electrodes. This means that the instantaneous velocity z-component is higher than the time-averaged one.

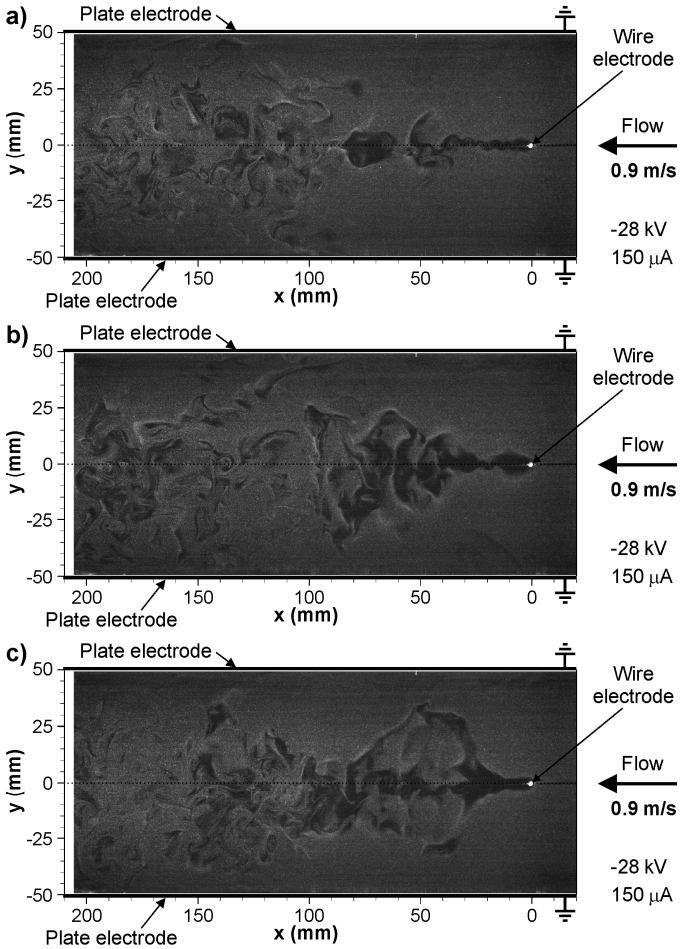

Fig. 16. Three instantaneous images (a, b and c) of the particle flow in the ESP. The applied voltage was -28 kV. The primary flow average velocity was 0.9 m/s. Exposure time: 6 ns.

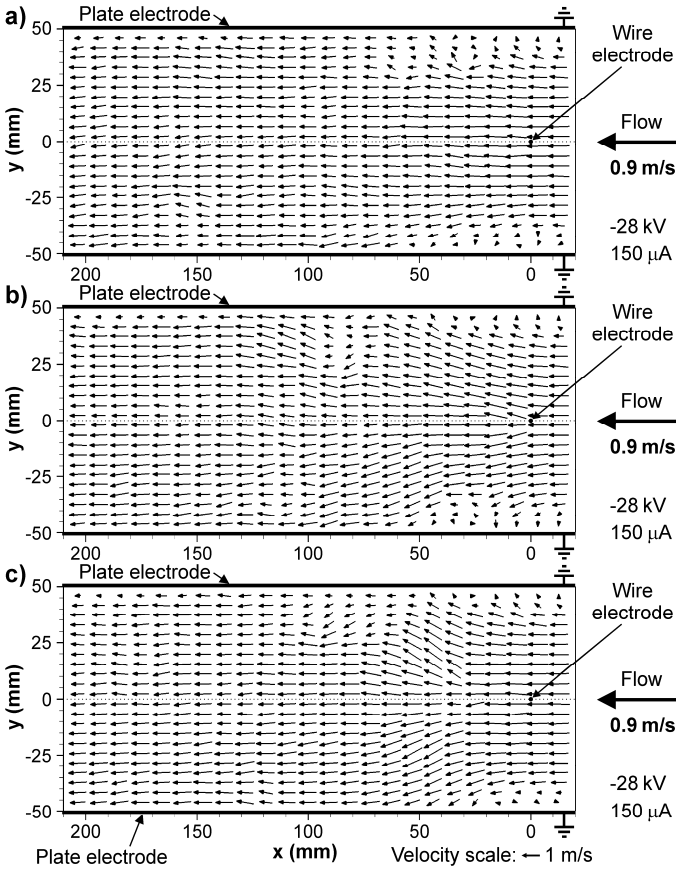

Fig. 17. Three instantaneous flow velocity fields (a, b and c) in the ESP. The applied voltage was -28 kV. The primary flow average velocity was 0.9 m/s.

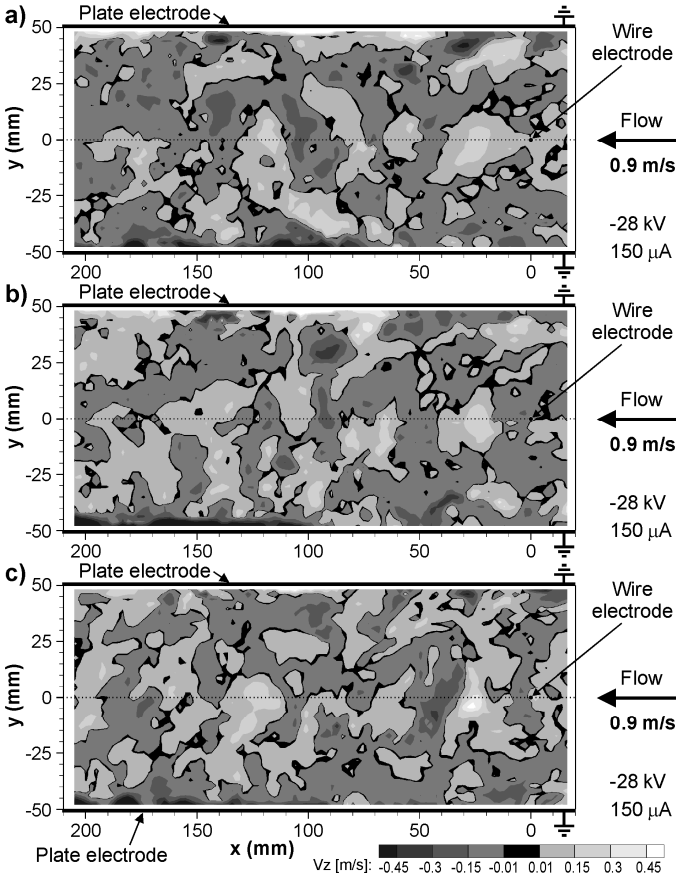

Fig. 18. Three instantaneous flow velocity z-component fields (a, b, c) in the ESP. Applied voltage: -28 kV. Primary flow average velocity: 0.9 m/s.

At a lower primary flow average velocity of 0.6 m/s (Ehd/Re^2 3.4) the particle flow disturbances, caused by the electric force, were stronger than those for the 0.9 m/s. The Karman vortex structure attempted to arise behind the wire electrode, but it was immediately scattered by irregular flow disturbances (see Figs. 19 a-c). At these conditions also the particle flow instabilities occurred near the plate electrodes. As it can be seen in corresponding instantaneous flow velocity fields (Figs. 20 a-c) irregular vortices arisen near the plate electrodes before the wire electrode. These vortices were scattered and floated by the primary flow. The velocity z-component fields (Fig. 21) are similar to those presented in Fig. 18. The flow velocity z-component structures are irregular. The velocity z-component reached values up to 0.35 m/s and more near the plate electrodes.

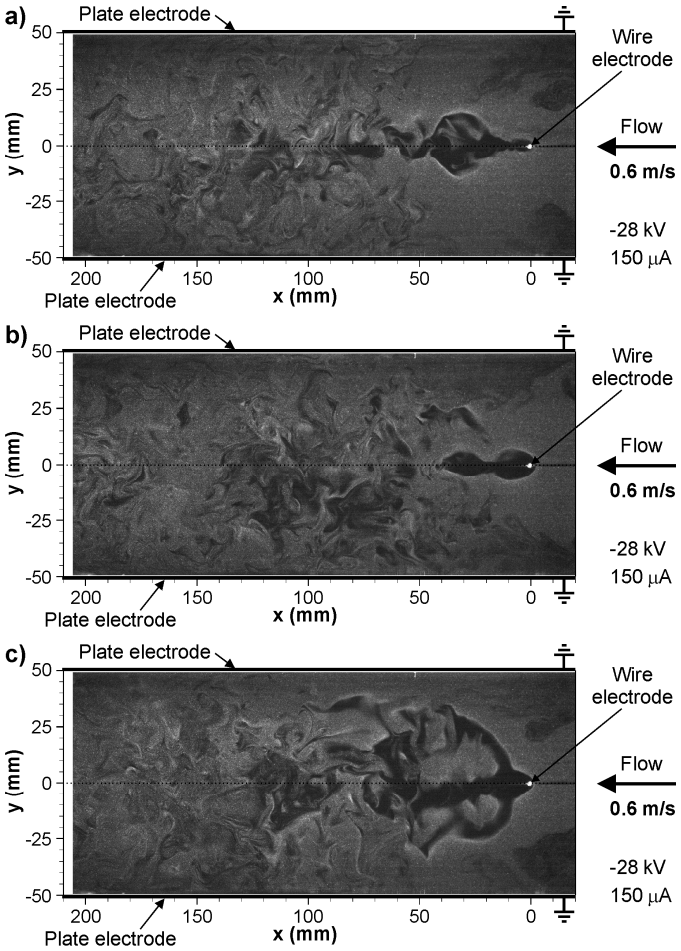

Fig. 19. Three instantaneous images (a, b and c) of the particle flow in the ESP. The applied voltage was -28 kV. The primary flow average velocity was 0.6 m/s. Exposure time: 6 ns.

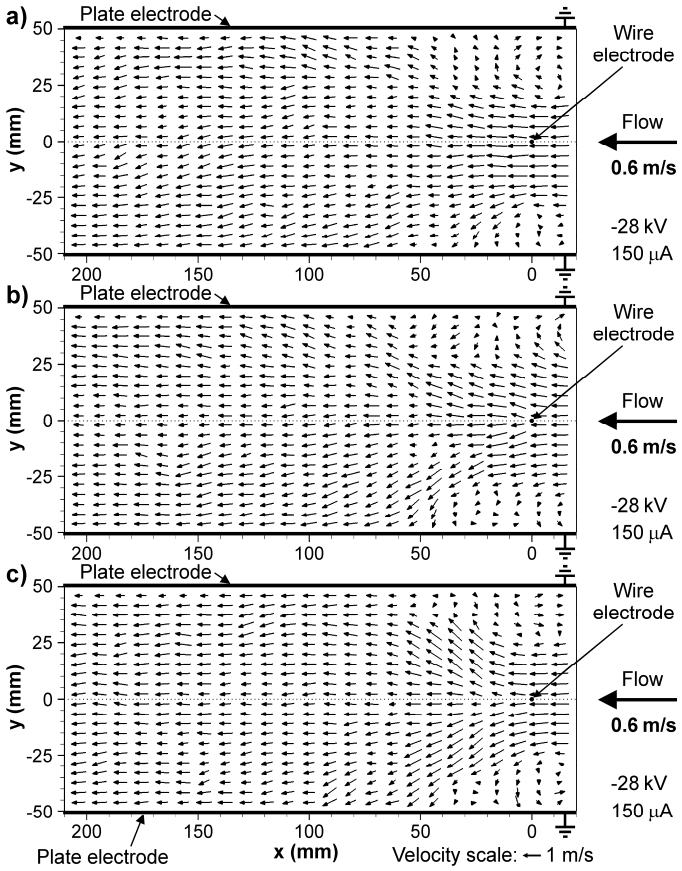

Fig. 20. Three instantaneous flow velocity fields (a, b and c) in the ESP. The applied voltage was -28 kV. The primary flow average velocity was 0.6 m/s.

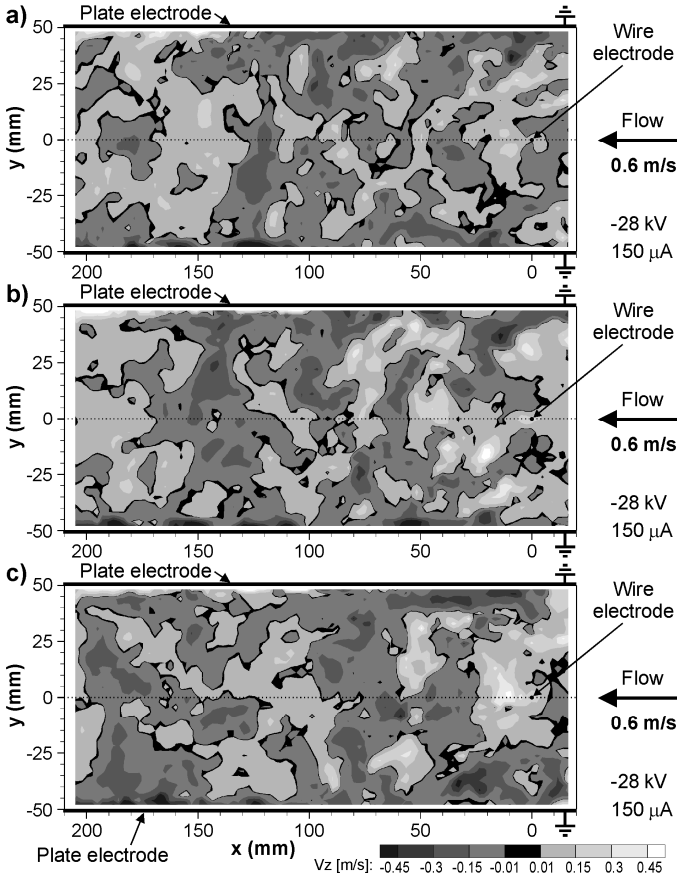

Fig. 21. Three instantaneous flow velocity z-component fields (a, b, c) in the ESP. Applied voltage: -28 kV. Primary flow average velocity: 0.6 m/s.

The instantaneous images of the particle flow and the corresponding instantaneous flow velocity fields measured in the ESP for the primary flow average velocity of 0.2 m/s (the Ehd/Re^2 ratio was 30.6) are presented in Figs. 22-24. One can see that the particle flow was very turbulent in the whole observation area. Any regular structure cannot be seen in the instantaneous images presented in Figs. 22 a-c. Also the flow velocity fields (Figs. 23 and 24) suggest that the particle flow in the ESP is turbulent and 3 dimensional when short time-interval are considered. However, some regularity in the particle flow patterns can be found from Figs. 23a-c. 50 mm downstream from the wire electrode and farther in the downstream, the velocity x-component near the plate electrodes reaches values up to 1 m/s (much higher than the primary flow average velocity). At the same time, the velocity x-component in the ESP duct centre reaches much lower values. At about 100 mm downstream from the wire electrode the velocity x-component becomes negative, i.e. the particles flow in the opposite direction to the primary flow direction. This counter-flow was already shown in the time-averaged results presented in Figs. 13 and 14. At the primary flow velocity of 0.2 m/s, the flow velocity z-component (Fig. 24) exhibit also very irregular structures, and with maximum velocity amplitude of about 0.45 m/s (i.e. higher than those at the primary flow velocity of 0.6 m/s and 0.9 m/s).

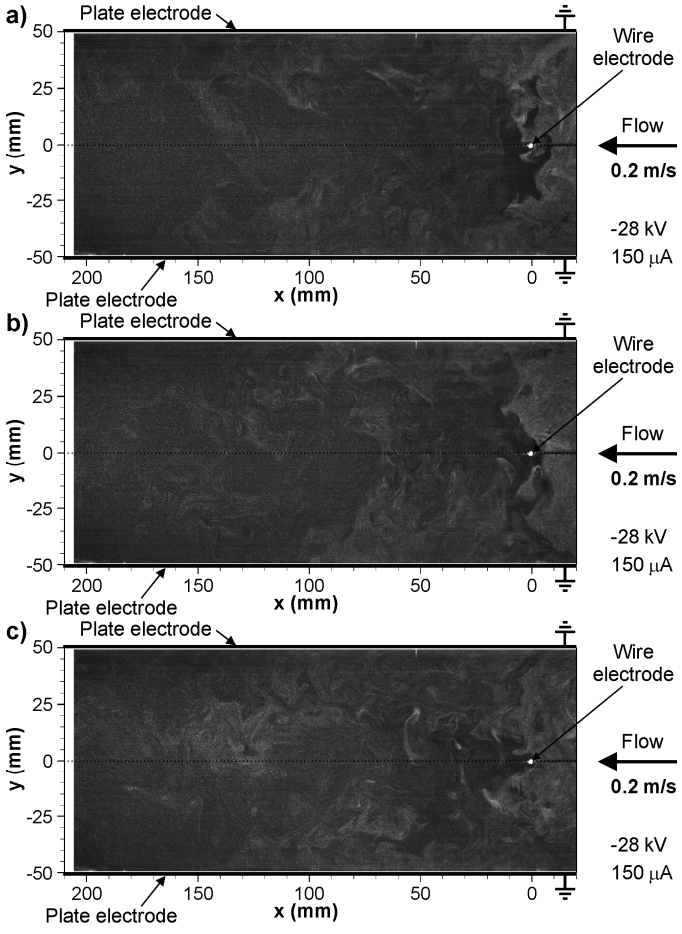

Fig. 22. Three instantaneous images (a, b and c) of the particle flow in the ESP. The applied voltage was -28 kV. The primary flow average velocity was 0.2 m/s. Exposure time: 6 ns.

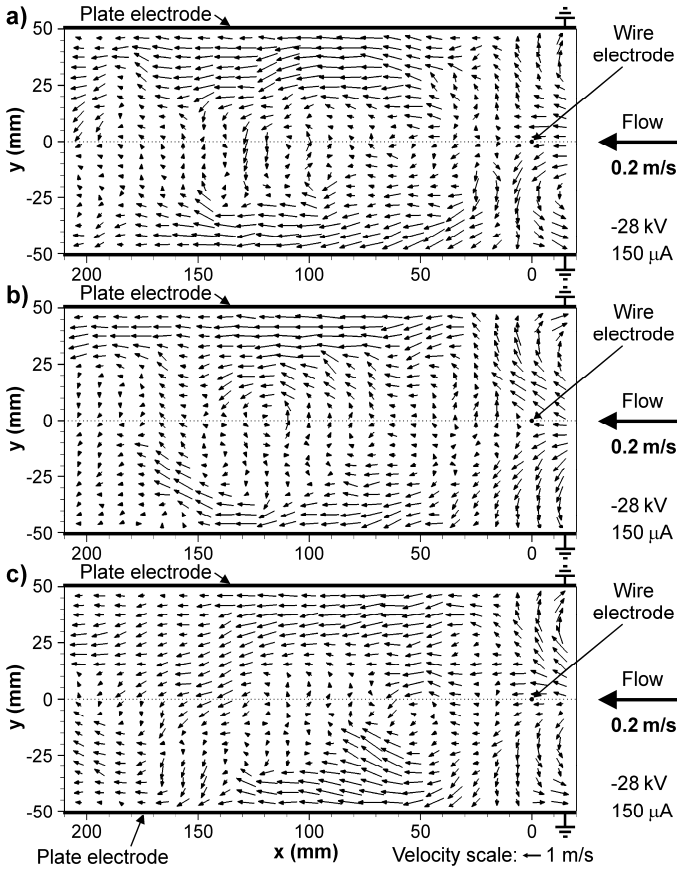

Fig. 23. Three instantaneous flow velocity fields (a, b and c) in the ESP. The applied voltage was -28 kV. The primary flow average velocity was 0.2 m/s.

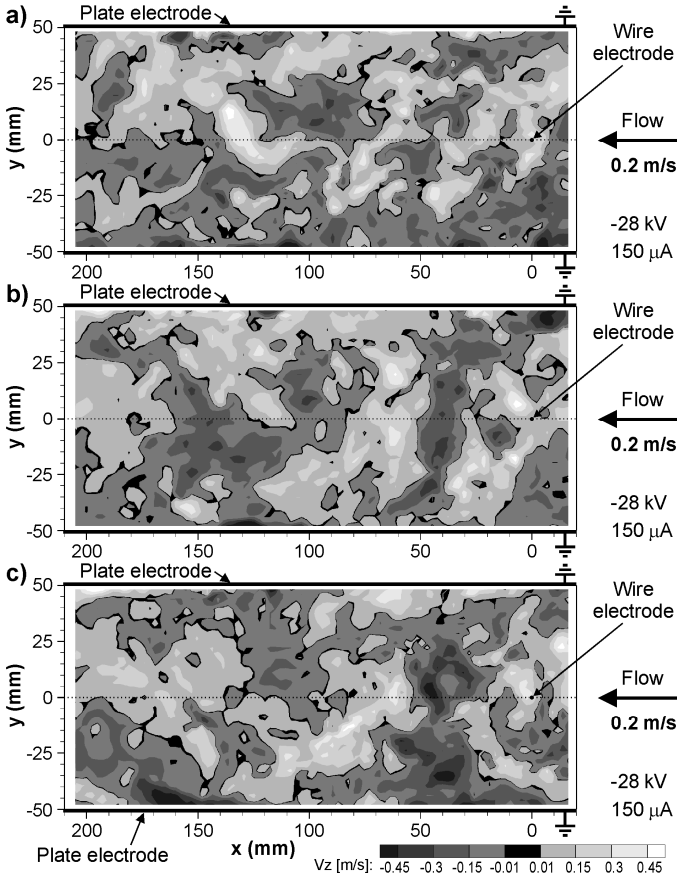

Fig. 24. Three instantaneous flow velocity z-component fields (a, b, c) in the ESP. Applied voltage: -28 kV. Primary flow average velocity: 0.2 m/s.

The standard deviations (SDs) of velocity z-component for the primary flow average velocities of 0.9 m/s, 0.6 m/s and 0.2 m/s are presented in Figs. 25, 26 and 27, respectively. As it can be seen from these figures, the velocity z-component SDs of reaches highest values in the wake behind the wire electrode. The SDs are higher for the primary flow velocity of 0.9 m/s (up to 0.3 m/s) than for 0.2 m/s (up to 0.25 m/s). However, at 0.9 m/s the particle flow in the ESP seems to be more stable in the majority of the observation area, and corresponding SDs of the velocity z-component is lower than 0.1 m/s. In comparison, at the primary flow velocity of 0.6 m/s and 0.2 m/s, the SDs of the velocity z-component reaches values up to 0.15 m/s and 0.2 m/s, respectively.

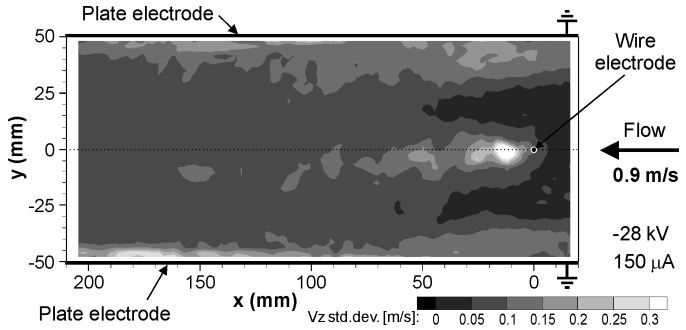

Fig. 25. Standard deviation of velocity z-component in the ESP. The applied voltage was -28 kV. The primary flow average velocity was 0.9 m/s.

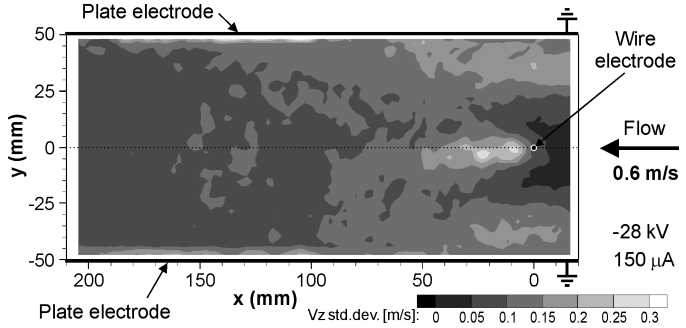

Fig. 26. Standard deviation of velocity z-component in the ESP. The applied voltage was -28 kV. The primary flow average velocity was 0.6 m/s.

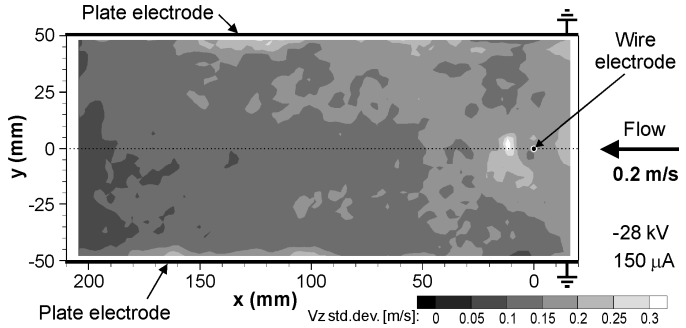

Fig. 27. Standard deviation of velocity z-component in the ESP. The applied voltage was -28 kV. The primary flow average velocity was 0.2 m/s.

IV. Conclusion

In this paper, the 3D PIV velocity field measurements in the midplane set along the ESP duct are presented. The obtained results showed that the time-averaged flow velocity in the z-direction (i.e. perpendicular to the primary flow direction) is low (lower than 0.05 m/s). This confirms the previous time-averaged results [10] indicating that the mean flow in the wide ESP is almost two-dimensional in terms of time-averaged observations. However, the analysis of instantaneous EHD flow images and velocity fields showed that the EHD flow is very turbulent with a relatively high instantaneous velocity z-component (up to 0.45 m/s). The high level of the velocity z-component standard deviation, calculated from the instantaneous velocity z-component fields, confirmed this observation. We expect that the flow turbulences are higher near the end-walls of the ESP. These results show that even in wide ESPs the EHD flow cannot be assumed to be 2-dimensional when its short-time flow behaviour is considered.

References

[1] D. Corbey, European Parliament resolution on the thematic strategy on air pollution (2006/2060(INI)).

[2] H. Krahmer, Report on the proposal for a directive of the European Parliament and of the Council on ambient air quality and cleaner air for Europe [COM(2005)0447 - C6-0356/2005 - 2005/0183(COD)] - Committee on the Environment, Public Health and Food Safety. (A6-0234/2006).

[3] A. Mizuno, "Electrostatic precipitation," IEEE Trans. Diel. Electr. Insul. 7 (2000) 615-624.

[4] P. Atten, F.M.J. McCluskey, A.C. Lahjomri, "The electrohydrodynamic origin of turbulence in electrostatic precipitators," IEEE Trans. Ind. Appl. 23 (1987) 705-711.

[5] T. Yamamoto, H. R. Velkoff, "Electrohydrodynamics in an electrostatic precipitator," J. Fluid Mech. 108 (1981) 1-18.

[6] G. L. Leonard, M. Mitchner, S. A. Self, "An experimental study of the electrohydrodynamic flow in electrostatic precipitators," J. Fluid Mech. 127 (1983) 123-140.

[7] J. Podliński, J. Dekowski, J. Mizeraczyk, D. Brocilo, J.S. Chang, "Electrohydro-dynamic gas flow in a positive polarity wire-plate electrostatic precipitator and the related dust particle collection efficiency," J. Electrost. 64 (2006) 259-262.

[8] J. Podliński, J. Dekowski, J. Mizeraczyk, D. Brocilo, K. Urashima, J.S. Chang, "EHD flow in a wide electrode spacing spike-plate electrostatic precipitator under positive polarity," J. Electrost. 64 (2006) 498-505.

[9] J. Podliński, A. Niewulis, J. Mizeraczyk, P. Atten, "ESP performance for various dust densities," J. Electrost. 66 (2008) 246-253.

[10] J. Podliński, R. Barbucha, J. Mizeraczyk, "EHD flow patterns in narrow and wide ESPs measured by 3D PIV method," in *Proc. 5eme Conf. Societe Francaise Electrostatique*, Grenoble, 2006, pp. 53-56.

[11] P. Atten, H.L. Pang, J.L. Reboud, J. Podliński, J. Mizeraczyk, "Turbulence generation by charged fine particles in electrostatic precipitators," in *Proc. ESA Annu. Meeting on Electrostatics 2007*, Laplacian Press, ISBN 1-885540-21-3, 2007, pp. 259-270.

[12] U. Kogelschatz, W. Egli, E.A. Gerteisen, "Advanced computational tools for electrostatic precipitators," ABB Review 4 (1999) 33-42.

[13] D. Brocilo, J.S. Chang, R. Godard, A. Berezin, "Numerical modelling of wire-pipe electrostatic precipitator for control of fine particulates," J. Aerosol Sci. 30-1 (1999) 855-856.

[14] H. Fujishima, Y. Morita, M. Okubo, T. Yamamoto, "Numerical simulation of three-dimensional electrohydrodynamics of spiked-electrode electrostatic precipitators," IEEE Trans. Diel. Electr. Insul. 13-1 (2006) 160-167.

[15] M. Raffel, Ch.E. Willert, J. Kompenhans, "Particle Image Velocimetry, A practical guide," Springer-Verlag Berlin Heidelberg, 2007.

[16] IEEE-DEIS-EHD Technical Committee, "Recommended international standard for dimensionless parameters used in electrohydrodynamics," IEEE Trans. Diel. Electr. Insul. 10-1 (2003) pp. 3-6.